Citation for final published version:

Andersen, Morten , Matthews, A, Vance, D, Bar-Matthews, M., Archer, C and Souza, G de 2018. A 10-fold decline in the Eastern Mediterranean thermocline overturning circulation during the last interglacial period. Earth and Planetary Science Letters 503 , pp. 58-67. 10.1016/j.epsl.2018.09.013

Publishers page: https://doi.org/10.1016/j.epsl.2018.09.013

A 10-fold decline in the deep Eastern Mediterranean thermohaline overturning circulation during the last interglacial period.

Authors: M Andersen[1,2*], A. Matthews[3], D. Vance[2], M. Bar-Matthews[4], C Archer[2], G de Souza[2]

[*]corresponding author: andersenm1@cardiff.ac.uk

[1]Cardiff University, School of Earth & Ocean Sciences, Park Place, Cardiff CF10 3AT, United Kingdom

[2]ETH Zürich, Institute of Geochemistry and Petrology, Department of Earth Sciences, Clausiusstrasse 25, 8092 Zurich, Switzerland

[3]Institute of Earth Sciences, Hebrew University of Jerusalem, 91904 Jerusalem, Israel

[4] Geological Survey of Israel, Jerusalem 95501, Israel

Keywords: Mediterranean, sapropels, uranium isotopes, molybdenum isotopes, last interglacial

word count: ~6500

Abstract

Present-day Mediterranean deep-waters are well oxygenated, but the episodic formation of organic-rich sediments (sapropels) indicates that this pattern was frequently perturbed in the past. Both high export productivity and disruption of the thermohaline circulation, leading to reduced deep-water ventilation, have been proposed to account for sapropel deposition and anoxia. The last interglacial sapropel S5 is considered one of the most strongly developed. Here, we apply the redox-sensitive Mo and U (elemental and isotope) systems to quantify the intensity of anoxic deep-water conditions in the Eastern Mediterranean Sea from ODP core 967 (2550 mbsl). Both U and Mo show strong authigenic enrichment, coupled to progressive increase in $\delta^{98}Mo_{auth}$ (1.2-1.8‰ to +2.0-2.3‰) and decrease in $\delta^{238}U_{auth}$ (+0.10‰ to -0.15‰) from the beginning to the end of S5, suggesting increasing water column euxinia and removal fluxes of Mo and U. Based on modern euxinic basins, we show that sedimentary $\delta^{238}U_{auth}$ can be used to derive estimates of water column U depletion and, ultimately, deep-water renewal rates. These principles are first tested on the modern Black Sea, which yields calculated deep-water renewal times of $830^{+690}/_{-500}$ years, in good agreement with independent estimates. Applying these principles to the end of S5 suggests bottom-water U depletion of ~50% and deep-water renewal times of $1030^{+820}/_{-520}$ years. The significantly slower deep-water renewal rates in the Eastern Mediterranean Sea compared to today (~100 years) would have played an important role in the formation of sapropel S5 and are consistent with the proposed suppression of overturning during the last interglacial, due to increased stratification resulting from higher riverine freshwater input under enhanced monsoon forcing.

1. Introduction

The Mediterranean overflow system and outflow into the Atlantic plays a major role in Atlantic Meridional Overturning Circulation (AMOC) (Johnson and Stevens, 2000; Rogerson et al., 2012). In its current configuration, the Mediterranean Sea is characterized by large-scale thermohaline circulation in which the relatively low salinity inflow from the Atlantic is converted via high evaporation in the Eastern Mediterranean Basin into an intermediate-depth saline outflow (Levantine Intermediate Water) (Malanotte-Rizzoli and Bergamasco, 1989; Pinardi and Masetti, 2000; Rohling et al., 2015) (Fig. 1). Such a circulation pattern leads to the formation of well-oxygenated deep-water in both the Eastern and Western Mediterranean basins, separated by the straits of Sicily. In the past, however, the periodic formation of organic carbon-rich sediments, termed sapropels, suggests that the redox state of deep-waters changed (e.g, Rossignol Strick, 1985; Rohling and Hilgren, 1991; Emeis et al, 1998; Emeis et al, 2000; Rohling et al., 2015).

Sapropels are associated with anoxic conditions in the deep ocean that allow the preservation of organic matter. Both higher export productivity, creating anoxia through enhanced consumption of oxygen, and disruption of oxygen supply via changes in the thermohaline circulation, have been proposed to account for the formation and preservation of organic matter (Rossingol-Strick, 1985; Rohling and Hilgen, 1991; Emeis et al., 2000; de Lange et al., 2008; Meyer and Kump, 2008). Pleistocene Mediterranean sapropels are unique sediments in that their periodicity is correlated with high northern hemisphere summer insolation during minima in the *ca.* 21 ka orbital precession cycle, and they are particularly well developed during interglacials. The resultant organic carbon-rich sedimentary deposits are important and useful analogs for such sediments in deeper time in Earth history. In this paper, we explore the validity of disrupted thermohaline circulation as a forcing factor in the creation of anoxia. Enhanced monsoon-driven freshwater runoff into the surface of the Eastern Mediterranean, through the Nile or transient North African rivers, or both, have all been put forward as important factors in the creation of less saline surface water layers. This, in turn, may have led to partial stratification of the water body and disruption of the thermohaline circulation system (Rossignol Strick et al., 1982; Emeis et al., 2000; Osborne et al., 2008; Bar-Matthews, 2014; Rohling et al., 2015). It is also recognized that some 'preconditioning' may have occurred, through the prior formation of anoxic deep-waters due to enhanced regional rainfall and sea level rise following glacial maxima (Grimm et al., 2015; Grant et al., 2016).

Geochemical proxies for redox conditions prevailing prior to and during sapropel formation, and following their termination as oxic conditions returned, include: organic biomarkers, elements sensitive to paleoproductivity and organic burial (e.g. barium) and redox-sensitive trace elements (RSTE, e.g. iron, manganese, vanadium, molybdenum, uranium) (Thomson et al., 1999; Cane et al., 2002; Rohling et al., 2006; de Lange et al., 2008; Almogi–Labin et al., 2009; Gallego-Torres et al, 2010). For instance, using a powerful combination of ^{14}C dating and RSTE profiles, de Lange et al. (2008) showed that basin-wide anoxic conditions prevailed during the formation of the latest (Holocene) sapropel, S1, at water depths > 1800m.

The stable isotope systems of the metals molybdenum and uranium, which fractionate during oxidation-reduction processes, can record distinctive isotope signatures during organic carbon-rich sedimentation (Barling et al, 2001; Arnold et al., 2004; Neubert et al, 2008; Weyer et al. 2008; Nägler et al., 2011; Andersen et al. 2014). In today's oxic oceans, the isotope composition of dissolved Mo (δ^{98}Mo +2.34‰, reported in delta-notation as δ^{98}Mo using the ^{98}Mo/^{95}Mo ratio normalized to NIST SRM 3134 standard +0.25 in parts per thousand; Nägler et al. 2014), dominated by the oxyanion molybdate species (MoO_4^{2-}), is thought to be fractionated relative to the Mo input to the ocean (δ^{98}Mo ~ +0.7‰; Archer & Vance 2008) mostly because of the loss of Mo adsorbed to manganese oxides (δ^{98}Mo ~ -0.7‰; Barling et al., 2001). In contrast, strongly euxinic (anoxic+sulfidic) water conditions result in near-quantitative uptake of Mo from seawater (either by scavenging to organic matter or through formation of a colloidal Fe-Mo-S species; Helz et al., 2011), driven by the transformation of molybdate to tetra-thiomolybdate (MoS_4^{2-}), with $MoS_4^{2-} >> MoO_4^{2-}$ when concentrations of H_2S are above 11 μMol (e.g. Neubert et al. 2008). This leads to organic carbon-rich sediments acquiring a δ^{98}Mo value very close to that of seawater, as has been recognized in organic carbon-rich sediments deposited in the euxinic deep Black Sea (Neubert et al., 2008; Nägler et al., 2011; Wegworth et al., 2018). Intermittent or weaker (H_2S concentrations <11 μMol) euxinic conditions, on the other hand, may lead to isotopically lighter Mo in sediments due to isotope fractionation during incomplete MoO_4^{2-} to MoS_4^{2-} transformation (Poulson-Brucker et al., 2012; Kerl et al., 2017). In sub-oxic to anoxic conditions, Mo isotope signatures intermediate between those of seawater and the oxic end-member may also reflect the importance of adsorption of isotopically light Mo species on iron oxides and pyrite (Goldberg et al., 2009). Indeed, δ^{98}Mo values much lower than modern seawater, and inferred weakly euxinic to anoxic conditions, have been observed in middle Pleistocene sapropels and in the most recent Holocene sapropel S1 at 2550 m water depth (Scheiderich et al., 2011; Azrieli-Tal et al., 2014). δ^{98}Mo minima from seawater during the early diagenesis of sapropel S1 in the Nile Fan have also been explained by Mo isotope fractionation during the kinetically-controlled particulate uptake of porewater thiomolybdate species (Matthews et al., 2017).

The mechanism for authigenic uranium enrichment in reduced sediments differs from that of molybdenum: while Mo removal primarily occurs in a euxinic water column, the major U uptake has been shown to, instead, occur within the reducing sediment environment, mediated by metal- and sulfate-reducing bacteria (Anderson et al., 1989; Lovley et al., 1991; McManus et al. 2006). The isotope system of the uranium parents ($^{238}U/^{235}U$, given in typical delta-notation as $\delta^{238}U$, which is the parts per thousand difference relative to the normalizing CRM-145 standard) has also been shown to respond to redox state as a result of significant positive isotope fractionation during the reduction of hydrated and complexed U(VI) ion to the largely immobile U(IV) ion (Stirling et al., 2007; Weyer et al., 2008; Andersen et al., 2017). Weyer et al. (2008) showed that $^{238}U/^{235}U$ from organic carbon-rich in Black Sea sediments was 0.4 to 0.8‰ higher than seawater, and subsequent studies have applied the $\delta^{238}U$ system as a paleoproxy for oceanic anoxia in ancient marine sediments (e.g. Montoya-Pino et al., 2010; Kendall et al, 2015). Andersen et al. (2014) showed that mass balance during the diffusion of uranium species through seawater and porewater constrains the $\delta^{238}U$ values preserved in sediment. This and subsequent studies (e.g. Noordmann et al., 2015; Holmden et al., 2016) have shown that mass-balance constraints at the sediment-water interface can lead to variable observed U isotope compositions, and that only a steady state situation involving U diffusion and uptake allows for quantitative interpretations of the $\delta^{238}U$ values in organic carbon-rich sediments.

Given the different mechanisms by which Mo and U isotopes respond to different redox situations, the combined isotope systematics of these elements offers enormous potential for quantifying and modeling oceanic processes during the formation of organic carbon-rich sediments, as recently demonstrated for the saline Lake Rogoznica, Adriatic Sea, Croatia (Bura-Nakić et al., 2018) and other modern and ancient organic-rich sediments (e.g. Kendall et al., 2015; Noordmann et al., 2015). Here we utilize coupled Mo and U isotope and RSTE systematics to study the evolution of redox conditions in the Eastern Mediterranean Sea during the formation of the last interglacial sapropel S5 (Eemian) period. We present data for the elemental and isotopic systems of Mo and U in sapropel S5 in a deep-water setting (2550m) with the ultimate aim of understanding the intensity of euxinia in deep-waters and quantify related slowdown in the thermohaline circulation of the Eastern Mediterranean Sea. Our study employs a new methodology based on U isotopes that can potentially be applied to other settings with density driven oceanic circulation. Thus, as part of the verification of the approach, we derive robust deep-water renewal times for the modern Black Sea.

2. Samples and setting

An extensive review of the Mediterranean climate, oceanography and periodic development of sapropels (particularly S1 and S5) is given by Rohling et al. (2015). Sapropel S5 was deposited during the last interglacial insolation maximum. It is considered to be the most intensely developed and most pristine of the more recent sapropels in the Eastern Mediterranean, Aegean and Levantine basins, with anoxia and euxinia extending up to as high as ~200 m below the sea surface (Rohling et al., 2006). It differs from sapropel S1, for which anoxic conditions only existed at open water depths of >1800m (deLange et al., 2008). In S1, Mo isotopes indicate that only weakly euxinic conditions developed in bottom waters (ODP Core 967D, 2550m depth; Azrieli-Tal et al., 2014). The samples of sapropel S5 (abbreviated "S5" in the following) were taken from ODP core 967C, drilled at a water depth of 2550m south of Cyprus, at the base of the northern slope of the Eratosthenes Seamount (Fig. 1). This study uses the dried and sieved <63 μm fraction of the samples analysed by Scrivner et al. (2004) for Nd isotope measurements in foraminifera (ODP 967C-H5, 70 to 110 cm), covering S5 and depths immediately above and below. Previous studies using the <63 μm fraction indicate that they provide a representative record of the elemental and isotope geochemistry of sapropels (Box et al., 2011; Azrieli-Tal et al., 2014). For core 967C-H5, benthic extinction occurs at 103 cm and benthic reoccurrence appears above approx. 74.5 cm. The S5 interval is defined to be within these boundaries (Cane et al., 2002). Total organic carbon (TOC) values determined for the same sample interval (by Emeis et al., 1998) show enrichments consistent with these boundaries (Supplementary Table), indicating that post-sapropel oxidation (oxidative burndown) did not significantly affect S5 at this core site. A 4.5 cm hiatus in the middle of S5 was proposed by Cane et al. (2002), terminating at 87 cm. By correlation to the Soreq cave $\delta^{18}O$ record, (Bar-Matthews et al., 2000) the S5 interval has been dated to 128-120 ka (Rohling et al., 2015).

3. Methods

Sample preparation and measurements were conducted at the facilities of the Bristol Isotope Group, University of Bristol, United Kingdom (U and Mo isotopes; clean laboratory chromatographic U separation), Hebrew University, Israel (clean laboratory chromatographic Mo separation), and Geological Survey of Israel (trace and major element chemistry).

3.1 Major and trace metal chemistry and analyses

Sample digestion for Mo separation and isotopic analysis was done in the clean laboratory at the Hebrew University of Jerusalem (HUJ). Samples were pyrolized at

800°C for approximately 12 hours to oxidize organic carbon. The pyrolized residue was then dissolved using HF, HNO_3 and HCl in the presence of H_2O_2. Trace and major element concentrations of 13 sediment samples were measured by low temperature plasma ashing of weighed amounts of sediments, followed by sodium peroxide sintering and chemical analysis at the Geological Survey of Israel using ICP-OES for major (Perkin Elmer Optima 3300) and ICP-MS for trace elements. Six samples were analyzed after pyrolysis and digestion by ICP-MS at HUJ. Based on the analysis of two geostandards (BHVO-1 and GIT-IWG IF-6) analytical errors (RSD) on single values for major and trace elements were within ±5%.

3.2 Molybdenum preparation and isotope analyses

Molybdenum separation for isotopic analysis was done using the procedure of Archer and Vance (2008), which sequentially elutes matrix elements, Cu, Fe and Mo. Prior to column chemistry, 1 ml of pre-cleaned anion exchange resin (Biorad anion resin AG MP-1 m, 100-200 mesh, chloride form) was loaded into 10 ml plastic Muromac® columns. The resin was then pretreated with 0.05M HNO_3, followed by 7M HCl containing 0.01% of 30% H_2O_2. Following elution, solutions were centrifuged to remove any particle contaminants, fluxed three times with 0.5 ml 15M HNO_3 and dried.

Molybdenum isotopic analyses were carried out at the University of Bristol, using a ThermoQuest Neptune instrument at low mass resolution ($M/\Delta M$ ~500). Solutions were introduced into the mass spectrometer in a 2% (v/v) HNO_3 solution by means of a CPI (Amsterdam, The Netherlands) PFA nebulizer and spray chamber fitted to a CETAC Aridus. Mass discrimination correction was achieved using a double spike, as described previously by others for Mo (Siebert et al., 2001) and using the specific procedure previously described for Zn (Bermin et al., 2006). All mass spectrometric errors were propagated through the double-spike calculation to obtain the final analytical uncertainty. Details of standards, calibration procedures, and error treatments are given in Azrieli-Tal et al. (2014). Replicate analyses of a multi-element standard (Me: Merck VI, 30 elements) run through the complete solution chemistry gave δ^{98}Mo = -0.03 ± 0.15‰ (2SD). All Mo isotope compositions for samples are corrected from the working CPI Mo ICPMS standard at Bristol (δ^{98}Mo Pacific Sea water =2.26 ± 0.03‰ (2SD); Archer and Vance, 2008) to the recommended NIST SRM 3134 δ^{98}Mo =0.25‰ (giving a δ^{98}Mo of 2.34‰ for seawater) (Nägler et al., 2014).

3.3 Uranium preparation and isotope analysis

Samples (10-50 mg) were dissolved in steps involving concentrated HNO_3, HF, HCl and H_2O_2. At the first dissolution step, in HNO_3 and HF, the IRMM3636 $^{236}U/^{233}U$ double spike was added, aiming for a $^{236}U/^{235}U$ of ~4. After heating, fluxing and subsequent drying, steps using heated 6 M HCl (x2) and a 7 M HNO_3 + 30% H_2O_2 mixture were completed, before samples were re-dissolved in 10 ml of 3 M HNO_3 in preparation for U-Teva chromatographic chemistry, following protocols in Andersen et al. (2014). Purified U fractions were dried and prepared for mass spectrometry in 2% (v/v) HCl aiming for 100-200 ppb U. Full procedural chemistry blanks were <20 pg U.

Uranium isotopic analyses were carried out at the University of Bristol, using a ThermoQuest Neptune instrument at low mass resolution (M/ΔM ~500) by means of a CPI (Amsterdam, The Netherlands) PFA nebulizer and spray chamber fitted to a CETAC Aridus. The set-up and measurement protocols were as outlined in Andersen et al. (2014; 2015). In brief, all Faraday cups were equipped with 10^{11} Ω resistors, apart from the cup for ^{238}U (10^{10} Ω). Measurements were conducted with "standard" sampler and "X" type skimmer cones. Typical sample ion beam intensities were ~1 nA for ^{238}U using ~50 ng U per analysis. Measurements of two unknowns were bracketed with the CRM-145 uranium standard, spiked in similar fashion as the unknowns. The in-house CZ-1 uraninite standard, processed through U-Teva chemistry and periodically measured in a similar fashion to the sediment samples, yielded δ^{238}U of –0.055±0.032 (±2S.D.) for ten repeats, in excellent agreement with previously published compositions for this standard (Stirling et al., 2007; Andersen et al., 2015). The external reproducibility for the CZ-1 standard is used as the uncertainty estimate for each of the unknowns.

4. Results

4.1 Sediment geochemistry

Several geochemical parameters allow the distinction of the S5 horizon from the sediments just above and below (Fig. 2, Table 1 and Supplementary Table). Both [TOC] (>2%) and [Ba] (2500-700 ppm) are higher during S5 than the surrounding sediments ([TOC] <1%, [Ba] 180-550 ppm). Concentrations of the RSTE [U] (13-37 ppm), [Mo] (25-140 ppm) and [V] (397-194 ppm) are highly elevated within S5, whereas the surrounding sediments have moderately elevated [U] (5-9 ppm), [Mo] (2-6 ppm) and [V] (166-74 ppm) compared to typical detrital background concentrations. The sediments surrounding S5 have δ^{98}Mo values ranging from +1.2 to +2.0‰, while within S5, δ^{98}Mo increases systematically from +1.0-+1.8‰ in the lower sections (102 to 90 cm) to +1.9-+2.3‰ in the upper sections (90 to 76 cm). The δ^{238}U compositions range from -0.35 to -0.22‰ in the sediments above and below the sapropel, while within S5, δ^{238}U values decrease systematically from approx. +0.10‰ in the lower sections (102 to 94 cm) to approx. -0.15‰ in the upper sections (94 to 76 cm). Normalizing [Fe], [U], [Mo] and [V] to [Al], a typical refractory element, reveals similar behavior to that of the absolute concentrations alone, with more elevated ratios during S5 than in the surrounding sediments, particularly in the later part of S5 (Fig. 3).

4.2 Authigenic Mo and U estimates in the sediments

A common method for estimating the authigenic fraction uses the measured [U] and [Mo] compared to [Al] (e.g. Algeo & Tribovillard, 2009), and normalizes these ratios to the estimates from detrital terrigenous siliciclastics, giving relative authigenic enrichment factors (EF) for U and Mo. Such EF estimates (see Table 1 for detrital Mo/Al and U/Al compositions used) suggest that the authigenic fraction dominates both the Mo and U budget during S5 (>94%) and that it also contributes a significant fraction in the surrounding sediments (72-93%). These values correspond to EFs of 21-101 for U (U_{EF}) and 35-327 for Mo (Mo_{EF}) during S5, and 4-16 for both in the surrounding sediments (Supplementary Table). The sediments surrounding S5 have relatively higher U_{EF} compared to the corresponding Mo_{EF}, while the Mo_{EF}/U_{EF} ratios towards the end of S5 are close to the present-day seawater Mo/U ratio. Comparing the sediments to the schematic marine water mass trajectories from physical and chemical controls on water masses of Algeo & Tribovillard (2009), they broadly follow a trajectory implying progression through open marine anoxic-sulfidic conditions (elevated Mo_{EF} over U_{EF}), although the sediments at the end S5 deviate from this trend and plot close to the Mo/U seawater ratio. There is a clear difference between the Mo_{EF} to U_{EF} trends in S5 compared to trajectories seen in Black Sea sediments (Algeo & Tribovillard 2009). The latter show a flatter trajectory (high enrichment factors with elevated U_{EF} over Mo_{EF}) that reflects Mo depletion in a highly restricted basin (see Fig 4a).

Authigenic U can furthermore be considered to belong to two main fractions: U from biogenic carbonates (which have low [Mo] and are not important for this element) and U incorporated from *in situ* uranium reduction within the sediments. Following procedures in Andersen et al. (2014), which assume that the [Ca] in bulk sediments is primarily from biogenic carbonates with ~1 ppm U content, the relative U contribution from this carbonate source to the authigenic fraction may also be estimated. This calculation shows that the biogenic carbonate U fraction constitutes <1% for S5 and <5% for surrounding sediments (Supplementary Table), so that the vast majority of U in these sediments is due to *in situ* reduction.

The isotope composition of the authigenic Mo and U fractions can also be estimated using the elemental concentrations in combination with Mo and U isotope compositions for the detrital terrigenous siliciclastic and (for U only) biogenic carbonate fractions. Here, values of $\delta^{238}U$ = -0.3‰ and $\delta^{98}Mo$ = 0‰ were used for the detrital terrigenous sediments and $\delta^{238}U$ = -0.4‰ for biogenic carbonate (Andersen et al. 2017; Kendall et al. 2017). Uncertainties on the authigenic composition were propagated by weighting the relative size of the detrital component following Andersen et al. (2014), see Table 1 for details. The dominance of the authigenic fraction for Mo and U generally leads to insignificant changes between the measured bulk and estimated authigenic $\delta^{238}U$ and $\delta^{98}Mo$ (Table 1). The only significant changes are for $\delta^{98}Mo_{auth}$ values from the sediments surrounding S5 (from +0.14 to +0.65‰ higher for $\delta^{98}Mo_{auth}$). Thus, whereas the bulk sediment $\delta^{98}Mo$ values of +1.4 to +2.1‰ broadly bracket the typical value of +1.6‰ in anoxic continental margin marine sediments (Poulson-Brucker et al., 2009), $\delta^{98}Mo_{auth}$ values (+1.6 to +2.4‰) shift toward the seawater $\delta^{98}Mo$ composition.

5. Discussion

All the measured sediments show signs of being deposited under oxygen-poor conditions (Figures 2 to 4). In the following, the sediments above and below S5 will be discussed first, before turning to the S5 sediments themselves, and how these results may be interpreted in terms of water column anoxia and deep-water renewal rates.

5.1 Mo and U uptake in the sediments surrounding S5

The sediments surrounding S5 are characterized by moderate U and Mo enrichment factors typical for an anoxic marine setting, accumulating relatively more authigenic U than Mo (see Fig. 4a). The observation of sediment anoxia prior to S5 fits well with previous suggestions of anoxia developing ~3000 year earlier than the actual S5 (Schmiedl et al., 2003), likely due to gradual Mediterranean surface water freshening associated with global sea-level rise (Rohling et al., 2015; Grant et al., 2016). The termination of S5 somewhere between sediments at 77 and 72 cm is distinctive and sharp for all proxies (Figures 2 and 3) and coincides with that indicated by [TOC] and [Ba], suggesting no significant post-depositional oxidative burn-down.

Both $\delta^{98}Mo_{auth}$ (+1.6 to +2.4‰) and $\delta^{238}U_{auth}$ (-0.35‰ to -0.17‰) in the sediments surrounding S5 are close to modern seawater values (+2.34‰ for $\delta^{98}Mo$ and -0.39‰ for $\delta^{238}U$). Authigenic $\delta^{238}U$ compositions near the seawater value have been observed in organic carbon-rich sediments from settings with periodically anoxic deep waters, presumably due to non-steady state diffusive U transport into, and removal within, sediments (e.g. Weyer et al., 2008; Andersen et al., 2014; Noordmann et al., 2015; Andersen et al., 2017). In such a setting, however, the δ^{98}Mo would be expected to be lower than the seawater composition, due to partial conversion of MoO_4^{2-} to MoS_4^{2-} under anoxic and possibly weakly euxinic water column conditions (e.g. Azriel-Tal et al., 2014). Instead, the Mo and U isotope compositions suggest near quantitative uptake of both authigenic U and Mo, but with relatively moderate U and Mo enrichment factors (Fig 4). This observation might suggest that uptake of authigenic Mo, as well as U, mainly occurs from pore-waters within the sediment. Uranium and Mo supply to these reducing porewaters is then limited by diffusion through a non-sulfidic penetration zone with finite depth, which leads to near-quantitative uptake for U and Mo at depths where pore-water sulfide concentrations are elevated enough to allow *in situ* precipitation of sulfide minerals like pyrite. The latter proposition could be supported by the relatively high sulfur content of all the sediments surrounding S5 (0.3 to 1.1 *wt%*; Supplementary Table). It should be noted that the highest $\delta^{98}Mo_{auth}$ values (those closest to seawater composition) in the non-sapropel sediments, are for the pre-sapropel samples. In contrast, post-sapropel sediments have slightly lower $\delta^{98}Mo_{auth}$ values (1.6 to 1.9‰), which may reflect incomplete Mo uptake from porewaters.

5.2 Molybdenum and U uptake in sediments within S5

Within S5, all studied proxies suggest well-developed anoxic conditions in the water column, leading to much higher U and Mo accumulation rates in these sediments compared to sediments surrounding S5 (Figures 2 and 3). None of the measured geochemical parameters in the sediments (Fig. 2) show any sign of the hiatus proposed by Cane et al. (2002) at around 87 cm (although no data are available at 88-90 cm).

However, the redox-sensitive proxies suggest a change from the early to the late part of S5. During the early stages of sapropel formation, the RSTE proxies (Fe, U, Mo, V) show a gradual increase above background values, consistent with developing anoxia. Further increases during the latter part of S5 (above 94 cm) are consistent with the development of increasingly euxinic conditions and higher removal rates of all the measured RSTE. While the high U/Al, Mo/Al and V/Al ratios tail off slightly towards the end of S5, the Fe/Al remains as high as in the sediments immediately beneath (Fig. 3).

The progressive increase in [Mo] and [U] during S5 is coupled with $\delta^{98}Mo_{auth}$ increase and $\delta^{238}U_{auth}$ decrease, suggesting progressively more quantitative uptake of both elements, with U and Mo isotope compositions moving towards the seawater compositions and the Mo_{EF}/U_{EF} moving towards the modern seawater ratio (Fig 4). There is a marked drop in $\delta^{98}Mo_{auth}$ values from the pre-sapropel sediment value of around +2.4‰ at 106.5 cm depth to approximately +1.2‰ in the first sapropel sample at 101.5 cm (Fig. 2). Given the corresponding increase in [Mo] from 6 to 25 ppm (Table 1), this drop could represent a shift from sulfidic porewater Mo uptake in the sediment to dominant uptake from anoxic ± sulfidic bottom waters. This transition could thus represent the point at which mechanisms for Mo and U uptake become decoupled.

The elevated $\delta^{98}Mo_{auth}$ values (+1.2‰ to +2.3‰) within S5 are in a similar range to those observed in sediments from modern euxinic basins (e.g. Black Sea, Cariaco Basin, Lake Rogoznica: Arnold et al., 2004; Neubert et al., 2008, Bura-Nakić et al., 2018), suggesting at least intermittent euxinic conditions in the water column that allow for the molybdate to tetra-thiomolybdate transformation. The progressive increase in $\delta^{98}Mo_{auth}$ from the beginning (+1.2-1.8‰) to the end (+2.0-2.3‰) of S5 could reflect a transition from weaker/intermittent to stronger/persistent euxinia, and more quantitative Mo removal. However, the effective molybdate to tetra-thiomolybdate transformation is equally affected by the time scale of transformation relative to that of deep-water renewal (Dahl et al., 2010). Thus, a decrease in deep-water ventilation may exert an equally important control on isotopically quantitative Mo sediment uptake (e.g. Bura-Nakic et al., 2018), as observed in the later section of S5. Of course, these processes are likely linked, as lower rates of inmixing of oxygenated waters may increase anoxia and euxinia in the deeper water column.

The high [U] and elevated $\delta^{238}U_{auth}$ (+0.1‰ to -0.15‰) during S5 are also similar to those observed in modern euxinic basins (e.g. Saanich Inlet, Black Sea, Cariaco Basin, Lake Rogoznica: Weyer et al., 2008; Andersen et al., 2014; Holmden et al., 2015; Bura-Nakić et al., 2018). Based on these modern analogs, the progressive decrease in $\delta^{238}U_{auth}$ during S5 is indicative of permanently anoxic bottom waters and steady-state diffusion-driven U removal into the reducing sediments, resulting in decreasing $\delta^{238}U_{auth}$ from increasing U depletion in the bottom waters (Andersen et al., 2014; Andersen et al., 2017). This U depletion is driven by the rate of U input versus that of removal and, therefore, also linked to the time scales of deep-water renewal.

An alternative explanation for the evolution of the RSTE and U-Mo isotope systematics during S5 could be related to an increasing addition of these elements from freshwater inputs. Matthews et al. (2017) discussed this issue for sapropel S1 in the Nile Fan and found that the effect of river Nile Mo input would not significantly lower seawater $\delta^{98}Mo$ above core site ODP 967. Also, the authigenic enrichments are orders of magnitude above potential riverine supply, and the Mo_{EF}/U_{EF} ratio during most of S5 is close to the modern seawater composition; these relationships would be fortuitous if riverine Mo and U supplies were significant. Furthermore, Mo and U freshwater input is very unlikely to concomitantly lead to waters with $\delta^{98}Mo$ values similar to seawater and the highest sedimentary $\delta^{238}U$ values, unless they were highly anomalous with respect to rivers measured to date (Archer & Vance, 2008; Andersen et al. 2017). Thus, during S5, both U and Mo isotope systems instead respond to the time scales of deep-water renewal and ventilation, despite the different removal mechanisms for Mo (precipitation within an anoxic–sulfidic water column) and U (diffusion into, and reduction within sulfidic sediments). This linked behavior is also indicated by the roughly linear correlation between the evolution of $\delta^{238}U_{auth}$ and $\delta^{98}Mo_{auth}$ (Fig 4b).

5.3 Estimates of U water column depletion from $\delta^{238}U$ in anoxic sediments

A compilation of globally distributed semi-restricted and euxinic basins shows that $\delta^{238}U_{auth}$ in the sediments exhibits a near-linear correlation with [U] depletion in basinal bottom waters relative to [U] in the oxic surface waters (Fig. 5). This observation is in keeping with the expectation of a linear relationship between sediment $\delta^{238}U$ and bottom-water $\delta^{238}U$ and U depletion derived from a diffusion-driven model of U loss into the sediments of euxinic basins with a fractionation factor of ~0.6% (see Andersen et al., 2014 and Bura-Nakić et al., 2018 for details). Although other U removal processes in the water column may occur (e.g. Rolison et al., 2017; Bura-Nakic et al., 2018), these have been shown to be of secondary importance compared to the *in situ* U reduction within sediments in euxinic basins (Bura-Nakic et al., 2018). This finding is supported by the good agreement between the regression line for modern-day restricted euxinic basins (Fig. 5) and that expected from the diffusion-driven U loss model discussed above. In the former, the range from 0% to 100% bottom-water U loss corresponds to $\delta^{238}U_{auth}$ of -0.42‰ and +0.19‰, respectively, whilst for the model this range is -0.40‰ to +0.20‰. Thus, bottom-water U depletion estimates agrees to within <3% when comparing these two methods.

The empirical correlation from modern-day settings can be used to quantify bottom-water U depletion in the Eastern Mediterranean at 2550 m during S5, by transforming $\delta^{238}U_{auth}$ sediment data to U depletion values (Fig. 5). Such an approach yields estimates of bottom-water U depletion from the beginning to the end of S5 that progressively increase from **12±24%** (96.5 cm) to **54±23%** (75.5 cm). The uncertainty of these estimates stem from the ±2S.D. uncertainty on the coefficients of the linear regression to the modern data in Fig. 5. It is important to note that the evolving bottom-water U depletions during S5 that can be obtained from sedimentary $\delta^{238}U_{auth}$ are not directly observable from [U] data or U/Al ratios (e.g. Fig. 3), as elemental proxies are also influenced by variable local U removal fluxes and sedimentation rates.

5.4 Using $^{238}U/^{235}U$ and deep-water renewal rates in semi-restricted anoxic basins: a concept and a test in the Black Sea

The sedimentary $\delta^{238}U_{auth}$ data can be used to provide constraints on the deep-water renewal rates during the formation of S5, with the help of a conceptual model. Here, a restricted basin is considered as a water column of unit area in which oxic surface and near-surface waters are separated by a chemocline from anoxic/euxinic waters below. The depth profile of [U] within the anoxic water column is set by the interaction between U loss to sediment at the base of the water column, and re-supply of U across the chemocline from U-rich oxic waters. At steady state, the total U depletion in the water column (relative to the U-rich oxic waters) is a function of the U loss/resupply rate. We can therefore apply our $\delta^{238}U_{auth}$-based estimates of bottom-water U depletion to calculate the rates of U resupply to the anoxic water column, i.e. the water renewal timescale τ, given by:

$$\tau = \frac{\Delta U}{\varphi_{sed}} \qquad \text{Eqn. 1}$$

where ΔU is the total-water-column U deficit (Fig. 6) and φ_{sed} is the U loss flux to sediment.

The simplest calculation of total water column U deficit is derived by assuming that U transport within the sub-chemocline water column takes place only due to small-scale mixing processes in the vertical direction, i.e. by turbulent diffusion. In this case, the resulting [U] profile will be linear, e.g. as observed in the Rogoznica sea-lake on the Croatian coast (Bura-Nakić et al., 2018), and the average U depletion over the entire anoxic water column will simply be one-half of the bottom-water U depletion estimate, derived from $\delta^{238}U_{auth}$ as calculated in Section 5.3. The value of ΔU can then be calculated as the difference in U inventory between that expected from conservative behavior of U, and the inventory calculated from the estimate of U depletion (Fig. 6):

$$\Delta U = U_{oxic} \cdot L - \frac{f_{bottom}}{2}\left(U_{oxic} \cdot L\right) \qquad \text{Eqn. 2}$$

where U_{oxic} is [U] in oxic surface waters above the chemocline, L is the depth of the water column below the chemocline, and f_{bottom} is the fractional depletion of U at the base of the water column derived from $\delta^{238}U_{auth}$. In addition to these parameters, in order to estimate the water renewal timescale τ we also require independent knowledge of the U loss flux to sediment φ_{sed} (Eqn. 1).

Before examining the Eastern Mediterranean during S5, we first assess this simple conceptual model using data from the modern Black Sea. The value of ΔU can be calculated from the known (but uncertain) parameters listed in Table 2. Additionally, the U loss flux to sediment is estimated to be 100 µg/cm^2/yr (Anderson et al., 1989; Andersen et al., 2014), with an uncertainty of ±25 µg/cm^2/yr. This U influx to sediments is similar to other modern euxinic restricted basins, taking into consideration the lower surface water [U] (~2.2 ppb) in the Black Sea relative to the open ocean [U] (~3.3 ppb) (e.g. ~150 ng/m^2/y of Cariaco Basin; Andersen et al., 2014). Based on these values, we calculate a deep-water renewal timescale of $\mathbf{830^{+690}/_{-500}}$ **years** (median and 97.5/2.5 percentile), in good agreement with independent estimates of Black Sea deep-water renewal rates (~400-1000 yr; *cf.* Algeo and Rowe, 2012). In our calculation, the uncertainty is propagated numerically by a Latin Hypercube sampling procedure (10^4 iterations) from the uncertainties on L, f_{bottom} and the φ_{sed} (see Eqns.1, 2 and Table 2). Note that any uncertainty arising from U depletion profiles that deviate from a perfect linear relationship with depth (e.g Black Sea, Anderson et al., 1989: Rolison et al., 2017) are implicitly incorporated into the empirical calibration regression line for estimating bottom-water U depletion from the sediment $\delta^{238}U_{auth}$ given in Figure 5.

5.5. Application to the Eastern Mediterranean during sapropel S5

We make the same calculation for the ODP 967 samples in the Eastern Mediterranean at the end of S5, as this is the time when our model assumptions (continuous euxinia and steady state) are most likely to be fulfilled. Performing the calculation for the sediment at 75.5 cm, with the lowest $\delta^{238}U_{auth}$, we obtain a deep-water renewal timescale of **$1030^{+820}/_{-520}$ years**. The slightly increased uncertainty relative to the Black Sea estimation results almost entirely from higher uncertainty on the depth of the S5 anoxic chemocline, for which there are variable estimates: based on benthic faunal proxies it has been suggested that anoxic (benthic azoic) conditions reached up to approximately 1000 m depth (Schmiedl et al., 2003; Capotondi et al., 2006), which is also approximately the saddle height between the Levantine and Ionian Sea. However, euxinic conditions up to the photic zone (~200 m) have also been proposed on the basis of organic biomarkers for S5 at site ODP 971 (~2000 m water depth) in the central Eastern Mediterranean Sea (Rohling et al., 2006). Similarly, Wegwerth et al (2018), infer water column euxinic conditions reaching up to a shallow photic zone redoxcline at the termination of S5 in the Black Sea. In our calculation, the chemocline is taken to be somewhere between 200 and 1400 m (800±600 m), to cover the large range in published estimates (see Table 2 for parameters and uncertainties).

Doing the same calculation for sediments at 96.5 cm (with highest $\delta^{238}U_{auth}$ closer to the S5 initiation), with U depletions estimate of $12^{+24}/_{-12}\%$, and with the same assumptions of continuous anoxia and steady state, we obtain deep-water renewal rates of **$340^{+385}/_{-325}$ years**. Yet, a finer-grained temporal analysis of the evolution of deep-water overturning rates across S5 is precluded by the uncertainties on input parameters, and by time constraints for reaching steady state. However, on a quantitative level, the decreasing $\delta^{238}U$ values from the start to the end of S5, coupled with $\delta^{98}Mo$ values moving towards the seawater composition, clearly suggest a progressive development of water mass restriction and increasing euxinia. Despite the relatively large uncertainty on the calculated deep-water renewal time, our calculations suggest a very significant slow-down in deep-water renewal above ODP 967 at the end of the last interglacial and during S5, compared to the deep-water overturning timescales of ~100 years in the modern Eastern Mediterranean (Rohling et al., 2015). Although these results are based on the ODP 967 site, U and Mo respond in relation to the deep-water circulation in the larger basin, thus reflecting the general systematics of the whole basin and a slowdown of the entire Eastern Mediterranean overturning system.

6. Implications for the Eastern Mediterranean during S5

The Mo-U isotopes and RSTE profiles across S5 in ODP 967 are consistent with development of deep-water stagnation and an anoxic chemocline with persistent euxinia leading to near-quantitative sedimentary uptake of Mo and a δ^{98}Mo value close to that of seawater. A similar pattern, involving the progressive move of sedimentary δ^{98}Mo values towards the seawater composition at the end of the last interglacial, has also been observed in the Black Sea (Wegwerth et al., 2018), suggesting a temporal link to the development of euxinia in the Eastern Mediterranean at the same time. The Eastern Mediterranean as a whole differs from the Black Sea in not being strongly physically restricted, though this specific site, situated on the flank of the Hellenic trench at the interface between the African and Eurasian plates, could be prone to more localized restriction. Nevertheless, strong restriction due to a 'bottleneck' situation like the Black Sea is an unlikely control on the development of bottom water euxinia in the Eastern Mediterranean Sea. Nor is there evidence of significant Mo depletion in the sapropel due to strong restriction (Fig. 4a). The observation in this study, based on the U isotope systematics, that there was a ten-fold decrease in deep-water renewal time relative to the modern, from ~100 to ~1000 years at the end of S5, is most consistent with a marked reduction in overturning in the Eastern Mediterranean Sea. This finding provides strong support for models proposing stratification of the Eastern Mediterranean Sea due to massive freshwater input (predominantly the River Nile) primarily related to enhanced monsoon forcing and increased westerly rainfall (Rossignol Strick et al., 1982; Emeis et al., 2003; Osborne et al., 2008; Bar-Matthews, 2014; Rohling et al., 2015, Grant et al., 2016).

The Mo isotope and RSTE data, furthermore, point to maximum euxinic conditions in the later stages of S5 development, consistent with a progressive slow-down of the overturning. It is notable that Holocene sapropel S1 shows peak development shortly after its initiation (Gallego-Torres et al, 2010; Azrieli-Tal et al., 2014; Matthews et al., 2017), whereas for S5 the strongest euxinic conditions occur in the latter part. Late-stage V/Al ratio maxima have also been noted for S5 in several Eastern Mediterranean ODP sites (Gallego-Torres et al, 2010), thus reinforcing that peak euxinic conditions occurred in the later stages across the whole basin. Modelling studies of Grimm et al. (2015) show that rapid S1 initiation occurred at the end of a long period (~6 ky) of deep-water stagnation resulting from post-deglaciation sea-level rise, while Grant et al. (2016) show that monsoon run-off was the main trigger for S5 formation. Since S5 was deposited following a glacial termination (MIS 6), it suggests that the extended period of prior deep-water stagnation modelled by Grimm et al. (2015) for S1 did not occur for S5. One scenario for the late peak euxinic conditions could involve a relative sea level drop from about +8 to about -20 msl (meters above mean sea level) during the S5 period (Grant et al., 2012). A sea level drop across S5 could limit the renewal of deep-water via Bernouilli aspiration over the straits of Sicily, necessary for normal circulation (Rohling et al., 2015) leading to decreasing deep-water overturning rates towards the later part of S5. The reasons for the relatively rapid collapse of S5 are also not clear. Gallego-Torres et al. (2010) proposed that rapid sapropel collapse and re-oxygenation of the deep Levantine basin is related to deep-water intrusion from the Northern Mediterranean Sea (Adriatic and Aegean seas). This suggestion, combined with a sharp reduction in monsoon flooding (Rohling et al., 2006), would be consistent with the view that deep-water overturn was related to the dual effects of Bernouilli aspiration and deep-water renewal (Rohling et al., 2015).

Finally we note that the quantitative estimates of deep-water renewal rates and estimates of euxinia in the water column for S5, based on the isotope systems of U and Mo, respectively, show how these proxies may provide more qualitative information on redox conditions in marine sediments than can be obtained from RSTE alone. These principles are also applicable to other settings, as shown with the calculated deep-water renewal rates for the Black Sea, and as such, can provide tools for further understanding the mechanisms leading to the deposition of other organic-carbon rich sediments in the past.

7. Acknowledgements

The research was supported by Israel Science Foundation grant 1140/12, ETH Zürich and the Swiss National Science Foundation, through grant 200020_165904. Olga Berlin of the Geological Survey of Israel is thanked for making the trace and major element analyses. We thank the Bristol Isotope Group for the hospitality, Elvira Bura-Nakić for discussions and reviews from Thomas Nägler and two anonymous reviewers that helped improving a previous version of the manuscript.

References

Algeo, T.J. and Rowe, H., 2012. Paleoceanographic applications of trace-metal concentration data. *Chem. Geol.*, **324**, 6-18.

Algeo, T.J., Tribovillard, N., 2009. Environmental analysis of paleoceanographic systems based on molybdenum–uranium covariation. *Chem. Geol.,* **268,** 211–225.

Andersen, M.B., Stirling, C.H., Weyer, S., 2017. Uranium isotope fractionation. *Reviews in Mineralogy and Geochemistry*, **82**, 799-850.

Andersen, M.B., Elliott, T., Freymuth, H., Sims, K.W., Niu, Y. and Kelley, K.A., 2015. The terrestrial uranium isotope cycle. *Nature*, **517**(7534), 356-359.

Andersen, M.B. Romaniello, S., Vance, D., Little, S.H., Herdman, R. and Lyons, T.W., 2014. A modern framework for the interpretation of 238U/235U in studies of ancient ocean redox. *Earth Planet. Sci. Lett.*, **400**, 184-194.

Anderson, R.F., Fleischer, M.Q., LeHurray, A.P., 1989. Concentration, oxidation state, and particulate flux of uranium in the Black Sea. *Geochim. Cosmochim. Acta,* **53**, 2215-2224.

Almogi-Labin, A., Bar-Matthews, M., Shriki, D., Kolosovsky, E., Paterne, M., Schilman, B., Matthews, A., 2009. Climatic variability during the last ~90ka of the southern and northern Levantine Basin as evident from marine records and speleothems. *Quat. Sci. Rev.*, **28**, 2882-2896.

Archer, C. and Vance, D., 2008. The isotopic signature of the global riverine molybdenum flux and anoxia in the ancient oceans. *Nature Geoscience,* **1**, 597-600.

Arnold, G.L., Anbar, A.D., Barling, J., Lyons, T., 2004. Molybdenum isotope evidence for widespread anoxia in Mid-Proterozoic oceans. *Science*, **304**, 87-90.

Azrieli-Tal, I., Matthews, A., Bar-Matthews, M., Almogi-Labin, A., Vance, D., Archer, C., Teutsch, N., 2014. Evidence from molybdenum and iron isotopes and molybdenum–uranium covariation for sulphidic bottom waters during Eastern Mediterranean sapropel S1 formation. *Earth Planet. Sci. Lett.*, **393**, 231-242.

Bar-Matthews, M., 2014. History of water in the Middle East and North Africa. In: Holland, H.D., Turekian, K.K. (Eds.), *Treatise on Geochemistry*, vol.14, second edition. Elsevier, Oxford, 109–128.

Bar-Matthews, M., Ayalon, A., Kaufman, A., 2000. Timing and hydrological conditions of Sapropel events in the Eastern Mediterranean, as evident from speleothems, Soreq cave, Israel. *Chem. Geol.*, **169**, 145–156.

Barling, J., Arnold, G.L., Anbar, A.D., 2001. Natural mass-dependent variations in the isotopic composition of molybdenum. *Earth Planet Sci. Lett.*, **193**, 447-457.

Bermin, J., Vance, D., Archer, C., Statham, P. J., 2006. The determination of the isotopic composition of Cu and Zn in seawater. *Chem. Geol.*, **226**, 280–297.

Box, M.R., Krom, M.D., Cliff, R.A., Bar-Matthews, M., Almogi-Labin, A., Ayalon, A., Paterne, M., 2011. Response of the Nile and its catchment to millennial-scale climatic change since the LGM from Sr isotopes and major elements of East Mediterranean sediments. *Quat. Sci. Rev.*, **30**, 431-442.

Bura-Nakić, E., Andersen, M.B., Archer, C., de Souza, G.F., Marguš, M., Vance, D., 2018. Coupled Mo-U abundances and isotopes in a small marine euxinic basin: Constraints on processes in euxinic basins. *Geochim. Cosmochim. Acta.,* **222**, 212-29.

Cane, T., Rohling, E.J., Kemp, A.E.S., Cooke, S., Pearce, R.B., 2002. High-resolution stratigraphic framework for Mediterranean sapropel S5: defining temporal relationships between records of Eemian climate variability. *Palaeogeogr. Palaeoclimatol. Palaeoecol.,* **183**, 87–101

Capotondi, L., Principato, M.S., Morigi, C., Sangiorgi, F., Maffioli, P., Giunta, S., Negri, A., Corselli, C., 2006. Foraminiferal variations and stratigraphic implications to the deposition of sapropel S5 in the eastern Mediterranean. *Palaeogeogr. Palaeoclimatol. Palaeoecol.*, **235**, 48–65.

Dahl, T.W., Anbar, A.D., Gordon, G.W., Rosing, M.T., Frei, R., Canfield, D.E., 2010. The behavior of molybdenum and its isotopes across the chemocline and in the sediments of sulfidic Lake Cadagno, Switzerland. *Geochim. Cosmochim. Acta.*, **74**, 144-163.

de Lange, G.J., Thomson, J., Reitz, A., Slomp, C.P., Speranza Principato, M., Erba, E., Corselli, C., 2008. Synchronous basin-wide formation and redox-controlled preservation of a Mediterranean sapropel. *Nature Geoscience,* **1**, 606–610.

Emeis, K.C., Sakamoto, T., Wehausen, R., Brumsack, H.J., 2000. The sapropel record of the eastern Mediterranean Sea—results of Ocean Drilling Program Leg 160. *Palaeogeog. Palaeoclimat. Palaeoecol.,* **158**, 371-395.

Emeis, K.C., Schulz, H.M., Struck, U., Sakamoto, T., Doose, H., Erlenkeuser, H., Howell, m., Kroon, D., Paterne, M., 1998. Stable isotope and alkenone temperature records of sapropels from sites 964 and 967: constraining the physical environment of sapropel formation in the eastern Mediterranean sea. In: Robertson, A.H.F., Emeis, K.C., Richter, C., Camerlenghi, A., Editors, *Proceedings of the Ocean Drilling Program, Scientific Results,* **160**, 309-331

Gallego-Torres, D., Martinez-Ruiz, F., de Lange, G. J., Jimenez-Espejo, F.J. Ortega-Huertas, M., 2010. Trace-elemental derived paleoceanographic and paleoclimatic conditions for Pleistocene Eastern Mediterranean sapropels. *Palaeogeog. Palaeoclimat., Palaeoecol.,* **293,** 76–89.

Goldberg, T., Archer, C., Vance, D., Poulton, S.W., 2009. Mo isotope fractionation during adsorption to Fe (oxyhydr)oxides. *Geochim. Cosmochim. Acta*, **73**, 6502–6516.

Grant, K.M., Rohling, E.J., Bar-Matthews, M., Ayalon, A., Medina-Elizalde, M., Ramsey, C.B., Satow, C. and Roberts, A.P., 2012. Rapid coupling between ice volume and polar temperature over the past 150,000 years. *Nature*, **491**(7426), p.744.

Grant, K.M., Grimm, R., Mikolajewicz, U., Marion, G., Ziegler, M., Rohling E.J., 2016. The timing of Mediterranean sapropel deposition relative to insolation, sea-level and African monsoon changes, *Quat. Sci Rev*, **140**, 125-141

Grimm, R., Maier-Reimer, E., Mikolajewicz, U., Schmiedl, G., Muller-Navarra, K., Adloff, F., Grant, K.M., Ziegler, M., Lourens, L.J., Emeis, K.C., 2016. Late glacial initiation of Holocene eastern Mediterranean sapropel formation. *Nat. Commun.,* DOI: 10.1038/ncomms8099.

Holmden, C., Amini, M., Francois, R., 2015. Uranium isotope fractionation in Saanich Inlet: A modern analog study of a paleoredox tracer. *Geochim. Cosmochim. Acta*, **153**, 202-215.

Johnson, J., and Steven, I., 2000. A fine resolution model of the eastern North Atlantic, between the Azores, the Canary islands, and the Gibraltar Strait. *Deep Sea Res. Part I*, **47**, 877-899.

Kendall, B., Dahl, T.W. and Anbar, A.D., 2017. The stable isotope geochemistry of molybdenum. *Reviews in Mineralogy and Geochemistry*, **82(1)**, 683-732.

Kendall, B., Komiya, T., Lyons, T.W., Bates, S.M., Gordon, G.W., Romaniello, S.J., Jiang, G., Creaser, R.A., Xiao, S., McFadden, K. and Sawaki, Y, 2015. Uranium and molybdenum isotope evidence for an episode of widespread ocean oxygenation during the late Ediacaran Period. *Geochim. Cosmochim. Acta*, **156**, 173-193.

Kerl, C.F., Lohmayer, R., Bura-Nakić, E., Vance, D., Planer-Friedrich, B., 2017 Experimental confirmation of isotope fractionation in thiomolybdates using ion chromatography and detection by multi-collector ICP-MS. *Anal. Chem.,* **89**, 3123-3129

Lovley, D.R., Phillips, E.J., Gorby, Y.A. and Landa, E.R., 1991. Microbial reduction of uranium. *Nature*, **350**(6317), 413-416

Malanotte-Rizzoli, P., Bergamasco, A., 1989. The circulation of the eastern Mediterranean. Part 1. *Oceanologica Acta*, **12**(4), 335-351.

Matthews, A., Azrieli-Tal, I., Benkovitz, A., Bar-Matthews, M., Vance, D., Poulton, S.W., Teutsch, N., Almogi-Labin, A., Archer, C., 2017. Anoxic development of sapropel S1 in the Nile Fan inferred from redox sensitive proxies, Fe speciation, Fe and Mo isotopes. *Chem. Geol.*, **475**, 24-39.

McManus, J., Berelson, W.B., Severmann, S., Poulson, R.I., Hammond, D.E., Klinkhammer, G.P., Holm, C., 2006. Molybdenum and uranium geochemistry in continental margin sediments: paleoproxy potential. *Geochim. Cosmochim. Acta*, **70**, 4643-4662

Meyer, K.L., Kump, L.R., 2008. Oceanic euxinia in earth history: causes and consequences. *Annu. Rev. Earth Planet. Sci.,* **36**, 251–288.

Montoya-Pino, C,, Weyer, S., Anbar, A.D., Pross, J., Oschmann, W., van de Schootbruuge, B., Arz, H.W., 2010. Global enhancment of ocean anoxia during Anoxic Oceanic Event 2: A quantitative approach using U isotopes. *Geology* **38**, 315-318.

Neubert, N., Nägler, T.F., Böttcher, M.E., 2008. Sulfidity controls molybdenum isotope fractionation in euxinic sediments: evidence from the modern Black Sea. *Geology* **36**, 775–778.

Nägler, T.F., Neubert, N., Böttcher, M.E., Dellwig, O., Schnetger, B., 2011. Mo isotope fractionation in pelagic euxinia: results from the modern Black and Baltic Seas. *Chem. Geol,.* **289**, 1–11.

Nägler, T.F., Anbar, A.D., Archer, C., Goldberg, T., Gordon, G.W., Greber, N.D., Siebert, C., Sohrin, Y., Vance, D., 2014. Proposal for an international molybdenum isotope measurement standard and data representation. *Geostand. Geoanal. Res.,* **38**, 149-151.

Noordmann, J., Weyer, S., Montoya-Pino, C., Dellwig, O., Neubert, N., Eckert, S., 2015. Uranium and molybdenum isotope systematics in modern euxinic basins: Case studies from the central Baltic Sea and the Kyllaren fjord (Norway). *Chem. Geol.*, **396**, 182-195.

Osborne, A.H., Vance, D., Rohling, E.J., Barton, N., Rogerson, M., Felloon, N., 2008. A humid corridor across the Shara for the migration of early modern humans out of Africa, 120,000 years ago. *Proc.Natl. Acad. Sci. USA,* **105,** 16444-16447.

Pinardi, N., and Masetti, E., 2000. Variability of the large scale general circulation of the Mediterranean Sea from observations and modelling: a review. *Palaeogeog. Palaeoclimat. Palaeoecol.*, **158,** 153–173.

Poulson-Brucker, R.L., McManus, J., Poulton, S.W., 2012. Molybdenum isotope fractionation observed under anoxic experimental conditions. *Geochem. J*, **46,** 201-209.

Poulson-Brucker, R.L., McManus, J., Severmann, S., Berelson, W.M., 2009. Molybdenum behavior during early diagenesis: Insights from Mo isotopes. *Geochem. Geophys., Geosyst.,* **10**(6).

Rogerson, M., Rohling, E.J., Bigg, G.R., Ramirez, J., 2012. Palaeoceanography of the Atlantic-Mediterranean Exchange: overview and first quantitative assessment of climatic forcing. *Rev. Geophys*. **50**, RG2003. http://dx.doi.org/10.1029/2011RG000376.

Rohling, E.J., Hilgen, F.J., 1991. The eastern Mediterranean climate at times of sapropel formation: a review. *Geologie en Mijnbouw,* **70**, 253-264.

Rohling, E.J., Hopmans, E.C., Sinninghe-Damsté, J.S., 2006.Water column dynamics during the last interglacial anoxic event in the Mediterranean (sapropel S5). P*aleoceanography* **21**, PA2018. http://dx.doi.org/10.1029/2005PA001237.

Rohling, E.J., Marino, G., Grant, K.M., 2015. Mediterranean climate and oceanography, and the periodic development of anoxic events (sapropels). *Earth-Sci.. Rev.*, **143**, 62–97.

Rolison, J.M., Stirling, C.H., Middag, R., Rijkenberg, M. J.A., 2017. Uranium stable isotope fractionation in the Black Sea: modern calibration of the $^{238}U/^{235}U$ paleo-redox proxy. *Geochim. Cosmochim. Acta*, **203**, 69-88.

Rossignol-Strick, M., 1985. Mediterranean Quaternary sapropels: an immediate response to of the African Monsoon to variation of insolation. *Paleogeog. ,Paleoclimatol. , Paleoecol.,* **49**, 237–265.

Rossignol-Strick, M., Nesteroff, V., Olive, P., Vergnaud-Grazzini, C., 1982. After the deluge: Mediterranean stagnation and sapropel formation. *Nature,* **295**, 105-110.

Scheiderich, K., Zerkle, A.L., Helz, G.R., Farquhar, J., Walker, R.J., 2010. Molybdenum isotope, multiple sulfur isotope, and redox sensitive element behavior in early Pleistocene Mediterranean Sapropels. *Chem. Geol.*, **279**, 134-144.

Schmiedl, G., Mitschele, A., Beck, S., Emeis, K.C., Hemleben, Ch., Schultz, H., Sperling, M., Weldeab, S., 2003. Benthic foraminiferal record of ecosystem variability in the eastern Mediterranean Sea during times of sapropel S5 and S6 deposition. *Palaeogeogr. Palaeoclimatol. Palaeoecol.*, **190**, 139-164.

Scrivner, A., Vance, D., Rohling, E.J., 2004. New neodymium isotope data quantify Nile involvement in Mediterranean anoxic episodes. *Geology*, **32**, 565–568.

Siebert, C., Nägler, T.F., Kramers, J.D., 2001. Determination of molybdenum isotope fractionation by double-spike multicollector inductively coupled plasma mass spectrometry. *Geochem. Geophys. Geosyst.,* **2**, 2000GC00124

Stirling, C.H., Andersen, M.B., Potter, E.-K., Halliday, A.N., 2007. Low temperature Isotope Fractionation of uranium. *Earth Planet. Sci. Lett.*, **264**, 208-225.

Thomson, J., Mercone, D., de Lange, G.J., van Santvoort, P.J.M., 1999. Review of recent advances in the interpretation of Eastern Mediterranean sapropel S1 from geochemical evidence. *Marine Geol.,* **153**, 77–89.

Wegwerth, A., Eckert, S., Dellwig, O., Schnetger, B., Severmann, S., Weyer, S., Brüske, A., Kaiser, J., Köster, J., Arz, H.W. and Brumsack, H.J., 2018. Redox evolution during Eemian and Holocene sapropel formation in the Black Sea. *Palaeogeog. Palaeoclimatol. Palaeoecol.*, **489,** 249-260.

Weyer, S., Anbar, A.D., Gerdes, A., Gordon, G.W., Algeo, T.J., Boyle, E.A., 2008. Natural fractionation of $^{238}U/^{235}U$. *Geochim. Cosmochim. Acta*, **72**, 345-359.

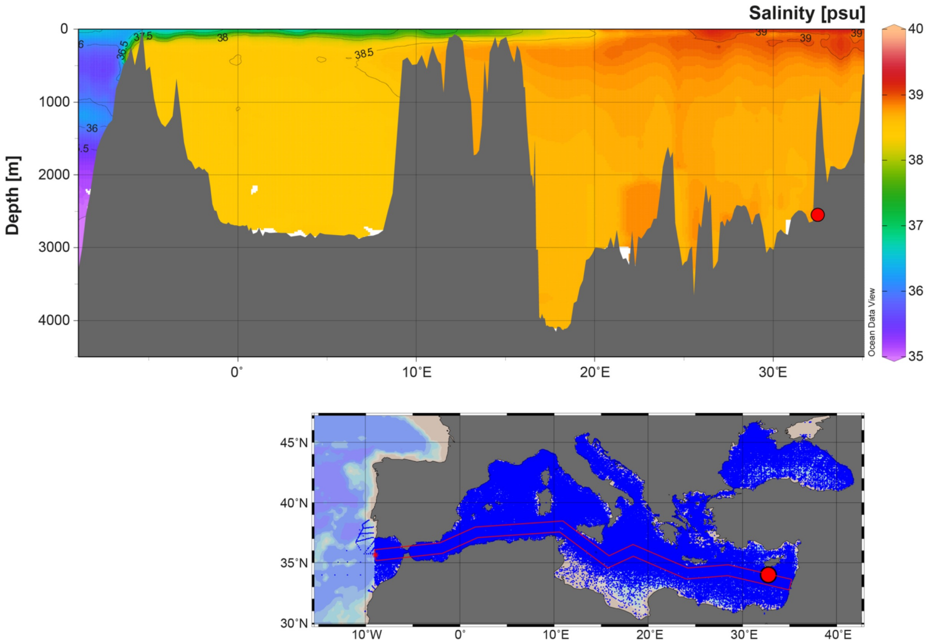

Figure 1. Vertical salinity profile (top) through the Mediterranean basin (bottom). The position of the studied core ODP 967 is marked with the red dot. Generated in Ocean Data View (https://odv.awi.de).

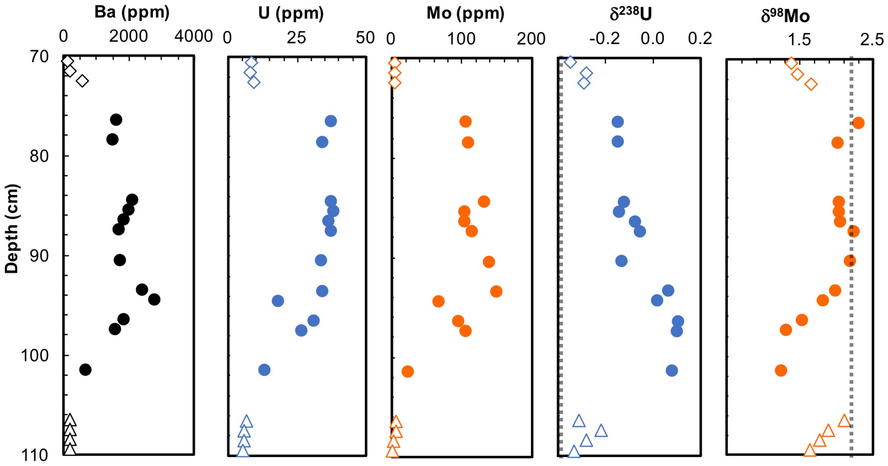

Figure 2. Core 967C-H5; depth in cm (110-70cm) vs. [Ba], [Mo], [U], δ^{98}Mo, δ^{238}U for post-S5 (open diamonds), S5 (filled circle) and pre-S5 (open triangles) samples. The open ocean isotope composition is shown as a dotted line for δ^{98}Mo (+2.34‰) and for δ^{238}U (-0.39‰) - the latter at the far left, close to the y-axis.

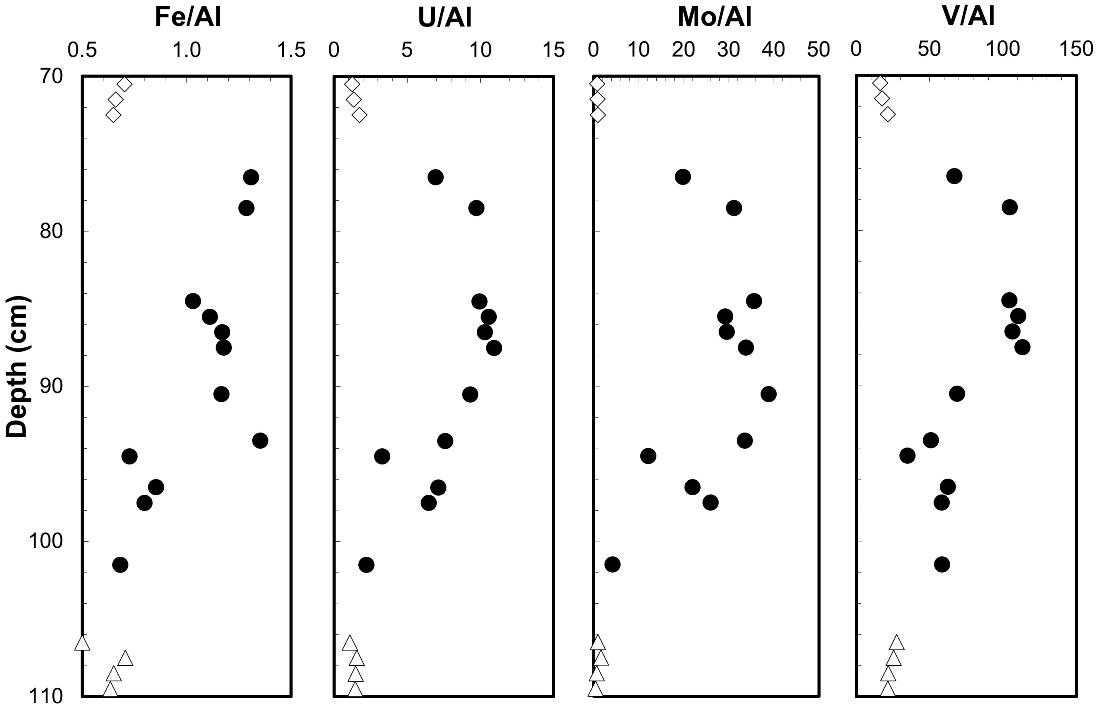

Figure 3. Ratios of Fe, U, Mo and V (ppm) vs Al (wt%), symbols as in Figure 2, show elevated values during S5 compared to before and after S5. All element to Al ratios also shows a general increase during S5. Although the last measured S5 sample at 76.5cm has as high Fe/Al as the previous sample, U/Al, Mo/Al and V/Al have all decreased.

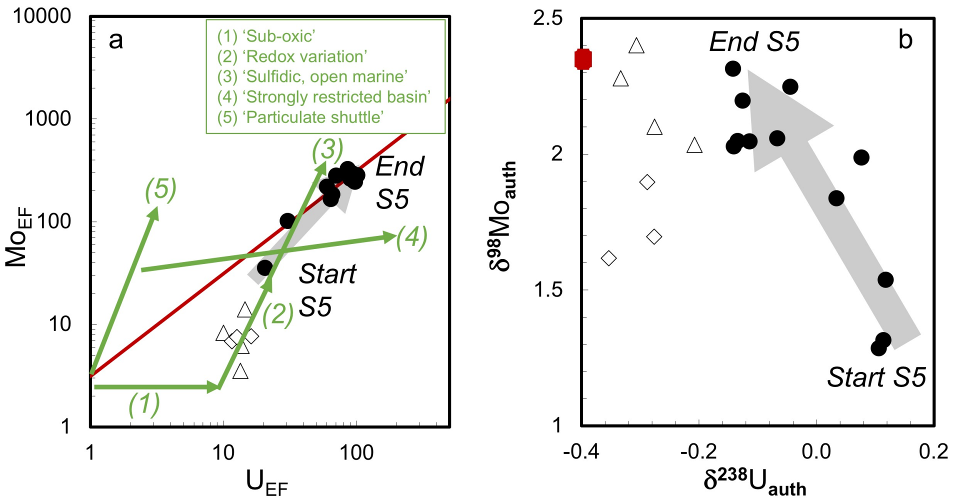

Figure 4. Cross-plots of authigenic U and Mo and their isotope systematics (symbols as in Figure 2). (a) The bold red line in (a) shows the Mo/U ratio in modern seawater. The green arrows show schematic evolution in enrichment factor trajectories based on physical and chemical controls on water masses, as presented by Algeo & Tribovillard (2009). The filled red symbol in (b) shows $\delta^{238}U$ and $\delta^{98}Mo$ compositions of modern open ocean seawater. Grey arrow shows evolution from beginning to end of S5. Linear regression through the S5 data gives y =-2.65x +1.84 with R^2 = 0.68.

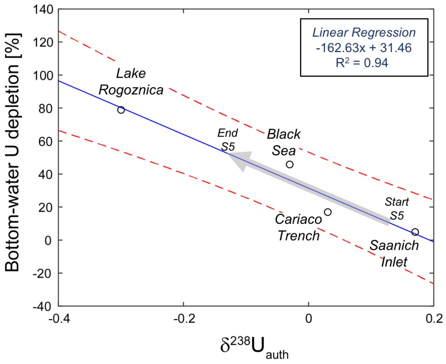
Linear Regression
-162.63x + 31.46
R² = 0.94
Lake Rogoznica
Black Sea
End S5
Start S5
Cariaco Trench
Saanich Inlet
Bottom-water U depletion [%]
140
120
100
80
60
40
20
0
-20
-40
-0.4
-0.2
0
0.2
δ238U auth

Figure 5. Cross-plot and linear regression (solid line, dashed lines are $2\sigma_{SD}$ uncertainty envelope) of authigenic δ^{238}U vs. bottom-water [U] depletion compared to the oxic surface (in percent) for a range of modern euxinic basins (Data are taken from Bura-Nakić et al., 2018, see this paper for data references). Note that data from Kyllaren Fjord (Noordmann et al., 2015), also reported in Bura-Nakić et al. (2018), has been left out from this calibration, since this site is affected by unusually high H_2S due to recent restriction of the fjord due to human activities. Grey arrow along the linear regression line shows the evolution of $\delta^{238}U_{auth}$ from the start to end of S5 (Fig. 1). Bottom-water U depletion above euxinic sediment samples can be calculated using the measured $\delta^{238}U_{auth}$ and the linear regression equation; $U_{depletion}$ (%)= $162.63*\delta^{238}U_{auth} + 31.46$.

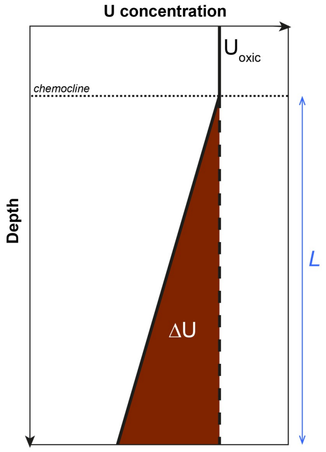

Figure 6. Schematic illustration of the creation of a water column U depletion profile (solid line) in a restricted basin with oxic surface waters separated from more stagnant anoxic/euxinic waters at depth. The total loss of U (ΔU) below the chemocline

compared to conservative U behavior (dashed line) can be calculated with knowledge of the length-scale of the water column below the chemocline (L), the [U] of the oxic surface waters above the chemocline (U_{oxic}) and the degree of U depletion at the base of the water column.

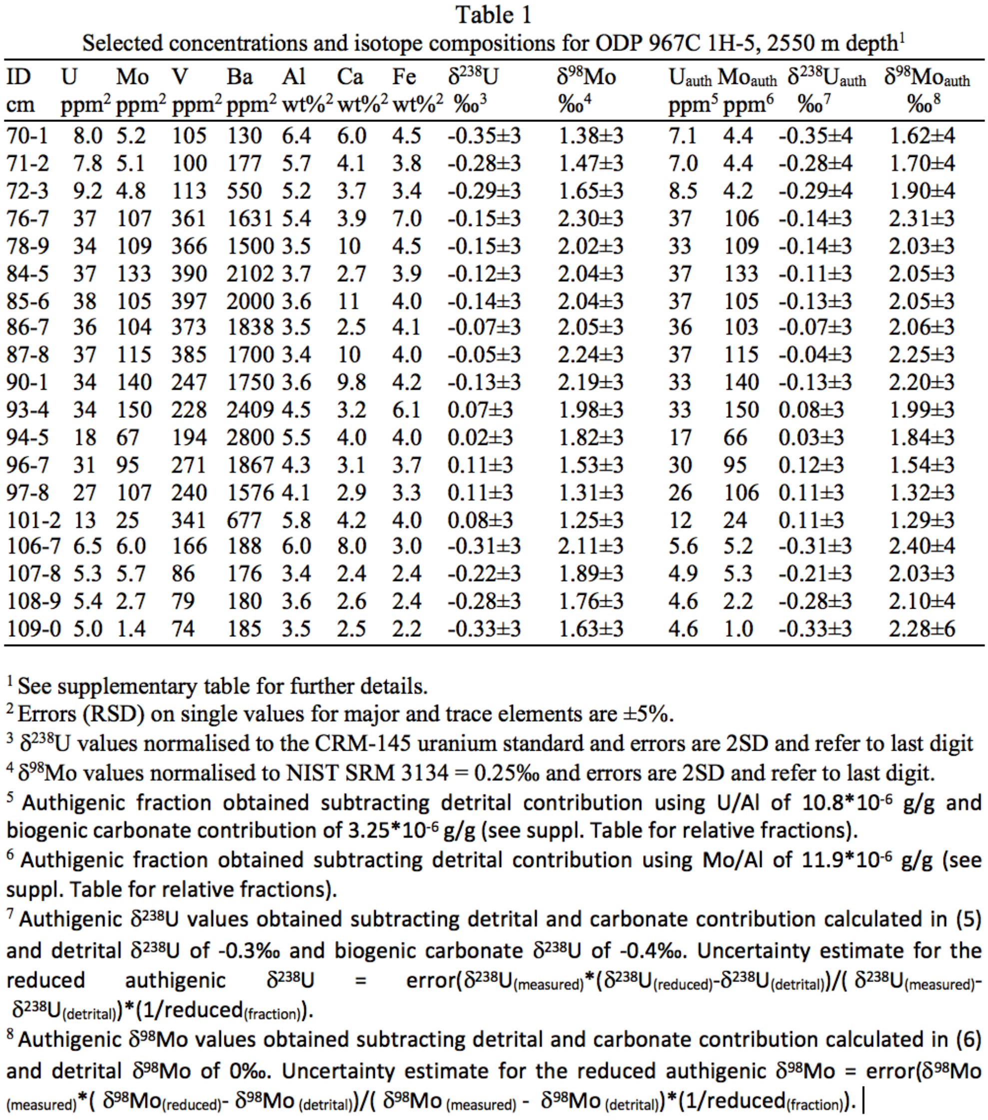

Table 1

Selected concentrations and isotope compositions for ODP 967C 1H-5, 2550 m depth[1]

ID cm	U ppm[2]	Mo ppm[2]	V ppm[2]	Ba ppm[2]	Al wt%[2]	Ca wt%[2]	Fe wt%[2]	$\delta^{238}U$ ‰[3]	$\delta^{98}Mo$ ‰[4]	U_{auth} ppm[5]	Mo_{auth} ppm[6]	$\delta^{238}U_{auth}$ ‰[7]	$\delta^{98}Mo_{auth}$ ‰[8]
70-1	8.0	5.2	105	130	6.4	6.0	4.5	-0.35±3	1.38±3	7.1	4.4	-0.35±4	1.62±4
71-2	7.8	5.1	100	177	5.7	4.1	3.8	-0.28±3	1.47±3	7.0	4.4	-0.28±4	1.70±4
72-3	9.2	4.8	113	550	5.2	3.7	3.4	-0.29±3	1.65±3	8.5	4.2	-0.29±4	1.90±4
76-7	37	107	361	1631	5.4	3.9	7.0	-0.15±3	2.30±3	37	106	-0.14±3	2.31±3
78-9	34	109	366	1500	3.5	10	4.5	-0.15±3	2.02±3	33	109	-0.14±3	2.03±3
84-5	37	133	390	2102	3.7	2.7	3.9	-0.12±3	2.04±3	37	133	-0.11±3	2.05±3
85-6	38	105	397	2000	3.6	11	4.0	-0.14±3	2.04±3	37	105	-0.13±3	2.05±3
86-7	36	104	373	1838	3.5	2.5	4.1	-0.07±3	2.05±3	36	103	-0.07±3	2.06±3
87-8	37	115	385	1700	3.4	10	4.0	-0.05±3	2.24±3	37	115	-0.04±3	2.25±3
90-1	34	140	247	1750	3.6	9.8	4.2	-0.13±3	2.19±3	33	140	-0.13±3	2.20±3
93-4	34	150	228	2409	4.5	3.2	6.1	0.07±3	1.98±3	33	150	0.08±3	1.99±3
94-5	18	67	194	2800	5.5	4.0	4.0	0.02±3	1.82±3	17	66	0.03±3	1.84±3
96-7	31	95	271	1867	4.3	3.1	3.7	0.11±3	1.53±3	30	95	0.12±3	1.54±3
97-8	27	107	240	1576	4.1	2.9	3.3	0.11±3	1.31±3	26	106	0.11±3	1.32±3
101-2	13	25	341	677	5.8	4.2	4.0	0.08±3	1.25±3	12	24	0.11±3	1.29±3
106-7	6.5	6.0	166	188	6.0	8.0	3.0	-0.31±3	2.11±3	5.6	5.2	-0.31±3	2.40±4
107-8	5.3	5.7	86	176	3.4	2.4	2.4	-0.22±3	1.89±3	4.9	5.3	-0.21±3	2.03±3
108-9	5.4	2.7	79	180	3.6	2.6	2.4	-0.28±3	1.76±3	4.6	2.2	-0.28±3	2.10±4
109-0	5.0	1.4	74	185	3.5	2.5	2.2	-0.33±3	1.63±3	4.6	1.0	-0.33±3	2.28±6

[1] See supplementary table for further details.

[2] Errors (RSD) on single values for major and trace elements are ±5%.

[3] $\delta^{238}U$ values normalised to the CRM-145 uranium standard and errors are 2SD and refer to last digit

[4] $\delta^{98}Mo$ values normalised to NIST SRM 3134 = 0.25‰ and errors are 2SD and refer to last digit.

[5] Authigenic fraction obtained subtracting detrital contribution using U/Al of 10.8*10-6 g/g and biogenic carbonate contribution of 3.25*10-6 g/g (see suppl. Table for relative fractions).

[6] Authigenic fraction obtained subtracting detrital contribution using Mo/Al of 11.9*10-6 g/g (see suppl. Table for relative fractions).

[7] Authigenic $\delta^{238}U$ values obtained subtracting detrital and carbonate contribution calculated in (5) and detrital $\delta^{238}U$ of -0.3‰ and biogenic carbonate $\delta^{238}U$ of -0.4‰. Uncertainty estimate for the reduced authigenic $\delta^{238}U$ = error($\delta^{238}U_{(measured)}$*($\delta^{238}U_{(reduced)}$-$\delta^{238}U_{(detrital)}$)/($\delta^{238}U_{(measured)}$-$\delta^{238}U_{(detrital)}$)*(1/reduced$_{(fraction)}$).

[8] Authigenic $\delta^{98}Mo$ values obtained subtracting detrital and carbonate contribution calculated in (6) and detrital $\delta^{98}Mo$ of 0‰. Uncertainty estimate for the reduced authigenic $\delta^{98}Mo$ = error($\delta^{98}Mo_{(measured)}$*($\delta^{98}Mo_{(reduced)}$- $\delta^{98}Mo_{(detrital)}$)/($\delta^{98}Mo_{(measured)}$ - $\delta^{98}Mo_{(detrital)}$)*(1/reduced$_{(fraction)}$).

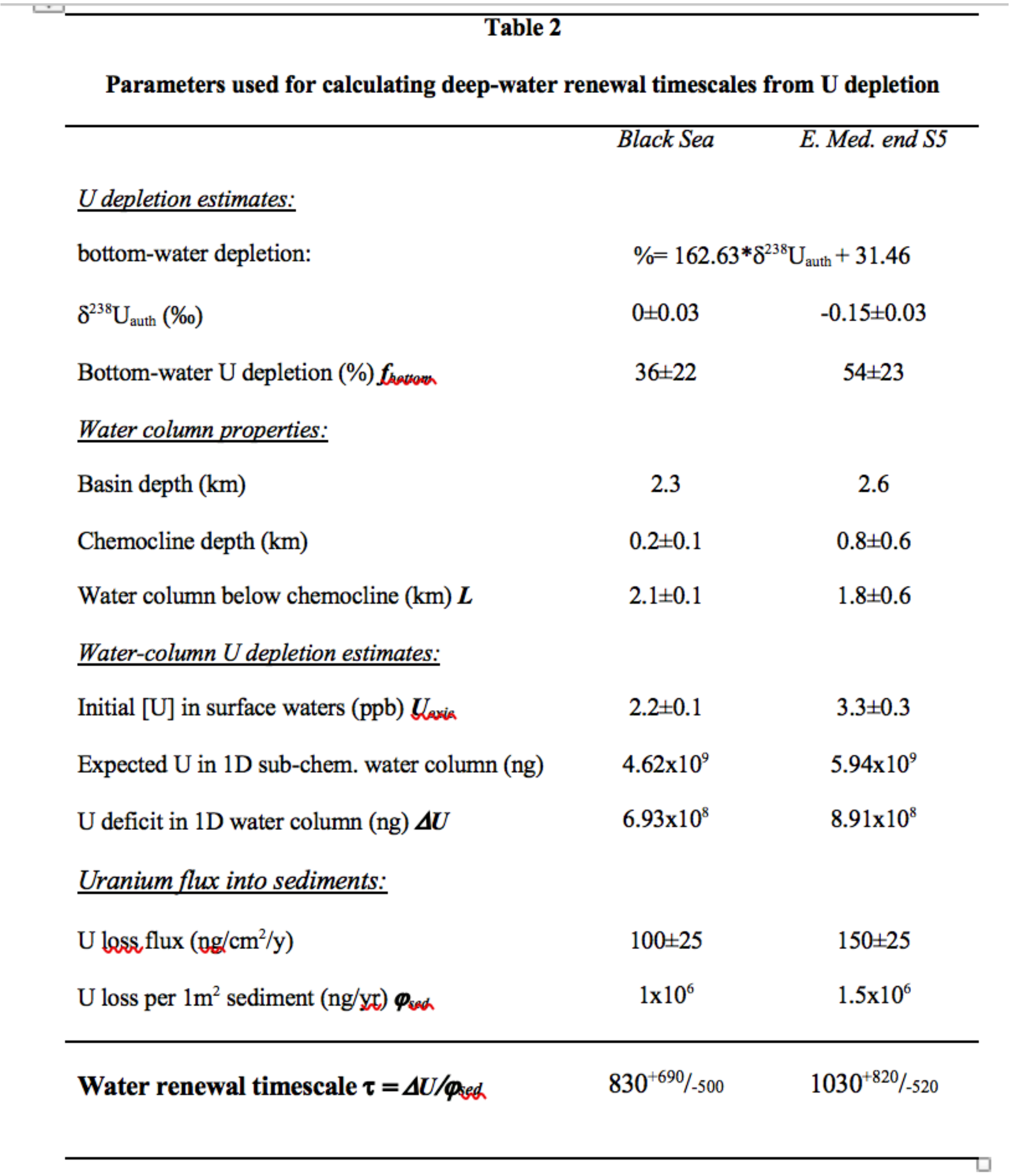

Table 2

Parameters used for calculating deep-water renewal timescales from U depletion

	Black Sea	*E. Med. end S5*
U depletion estimates:		
bottom-water depletion:	$\% = 162.63 * \delta^{238}U_{auth} + 31.46$	
$\delta^{238}U_{auth}$ (‰)	0 ± 0.03	-0.15 ± 0.03
Bottom-water U depletion (%) f_{bottom}	36 ± 22	54 ± 23
Water column properties:		
Basin depth (km)	2.3	2.6
Chemocline depth (km)	0.2 ± 0.1	0.8 ± 0.6
Water column below chemocline (km) L	2.1 ± 0.1	1.8 ± 0.6
Water-column U depletion estimates:		
Initial [U] in surface waters (ppb) U_{axis}	2.2 ± 0.1	3.3 ± 0.3
Expected U in 1D sub-chem. water column (ng)	4.62×10^9	5.94×10^9
U deficit in 1D water column (ng) ΔU	6.93×10^8	8.91×10^8
Uranium flux into sediments:		
U loss flux (ng/cm^2/y)	100 ± 25	150 ± 25
U loss per 1m^2 sediment (ng/yr) φ_{sed}	1×10^6	1.5×10^6
Water renewal timescale $\tau = \Delta U / \varphi_{sed}$	$830^{+690}/_{-500}$	$1030^{+820}/_{-520}$